THE GEOLOGICAL SOCIETY OF AMERICA®

A probabilistic analysis of meteorically altered $\delta^{13}C$ chemostratigraphy from late Paleozoic ice age carbonate platforms

Blake Dyer[1,2], John A. Higgins[2], and Adam C. Maloof[2]
[1]Lamont-Doherty Earth Observatory, Columbia University, 61 Route 9W, Palisades, New York 10964, USA
[2]Department of Geosciences, Princeton University, Guyot Hall, Washington Road, Princeton, New Jersey 08544, USA

ABSTRACT

The stratigraphic expression of meteoric diagenesis in carbonates is a glimpse into the weathering, fluid transport, and biological productivity of the ancient near-surface terrestrial environment. To infer this environmental information, we use a probabilistic approach to merge an isotope-based reactive transport model with chemostratigraphic data from carbonates that were subaerially exposed during an expansion of the late Paleozoic ice age in the middle Carboniferous. The rate of carbon flowing through the carbonate platform relative to the rate of carbon reacting between mineral and fluid phases controls the length scale, curvature, and magnitude of the diagenetic carbon isotope profiles. The ratio of advection to reaction is determined for seven stratigraphic sections, and the advection rate is used to estimate the minimum carbonate weathering associated with each profile. These carbonate weathering rates extrapolated over the expansive shallow carbonate platforms of the middle Carboniferous indicate that glacioeustatic fall may have caused a 20%–50% increase in the dissolved $CaCO_3$ flux to the ocean. The complex feedbacks among carbonate weathering and accumulation, atmospheric pCO_2, glacioeustasy, and passive margin subsidence may have played an unexplored role in the glacial-interglacial climate dynamics of the late Paleozoic ice age.

INTRODUCTION

The sedimentary record of seawater chemistry forms a basis for our understanding of the coevolution of the atmosphere, lithosphere, and biosphere through deep time. Chemical sediments, such as carbonates, precipitate from the water column and form layered archives from which secular changes in seawater chemistry are inferred (e.g., Hayes et al., 1999; Veizer et al., 1999). These carbonate sediments often are deposited in a shallow environment that can be subjected to diagenetic reactions during local sea-level fall or uplift (James and Choquette, 1984). Without proper identification, this diagenetic window may lead to false inferences about seawater chemistry as some of the chemical information imparted during the precipitation from seawater is erased (Allan and Matthews, 1982; Swart and Eberli, 2005).

When sea level falls and carbonate platforms are exposed, meteoric fluids infiltrate the pore space of the carbonate platform (Thrailkill, 1968; Matthews, 1974; Bögli and Schmid, 1980). These fluids first pass through an ephemerally wet vadose region in the upper part of the exposed rocks. A persistently water-saturated phreatic zone beneath this vadose zone records the long-term chemical reactions between the flowing meteoric waters and carbonate sediments. In this zone, the transfer of carbon from the atmosphere and soil to the underlying freshwater phreatic realm can lead to a carbon isotopic excursion in $\delta^{13}C_{carb}$ (Allan and Matthews, 1982; Lohmann, 1988). If this diagenetic product is a function of weathering, fluid transport, and biological productivity, then chemostratigraphic data from the altered rocks provide a window into the ancient near-surface terrestrial critical zone.

A vast karst terrain from the middle Carboniferous is exposed in the western United States, and a major subaerial exposure surface overlying those rocks is associated with carbon isotope excursions (Dyer et al., 2015). This paper merges observations of $\delta^{13}C$ data from this major exposure surface with a numerical fluid-mineral reactive transport model to indicate that the variations in the length scale and magnitude of the isotopic excursions can be explained entirely by changes in the ratio of carbon advecting through the rocks to carbon reacting with the rocks during meteoric diagenesis. Coupling an isotope-based reactive transport model with high-resolution isotopic data offers a way to quantify the extrinsic environmental forcings that created this archive of an otherwise unpreserved ancient terrestrial environment. This work is a step toward that goal, and demonstrates a framework for extracting paleoenvironmental information from any isotopic profiles associated with meteoric diagenesis throughout geologic time.

FORWARD REACTIVE TRANSPORT MODEL

A representative forward model for meteoric diagenesis must capture persistent isotopic exchange between mineral phases and a fluid flowing through the pore space of the rock. In detail, this process depends on fluid carbonate chemistry and small-scale fluid dynamics arising from complex permeability networks. However, a simpler modeling approach may be sufficient to capture the first-order isotopic expression of meteoric diagenesis in the phreatic zone. The dissolution of carbonate minerals in the upper vadose zone buffers the carbonate chemistry of the fluids entering the phreatic zone, where isotopic exchange between fluids and rocks clearly persists (Allan and Matthews, 1982; Lohmann, 1988; Swart and Eberli, 2005). Modern pore-water chemistry suggests that this diagenesis occurs near or at equilibrium in the phreatic zone (Plummer et al., 1976; Budd, 1988; Whitaker and Smart, 2007). These observations justify a modeling approach where the diagenetic fluids have carbonate chemistry near equilibrium, and the diagenetic reaction can be prescribed as continuous small-scale dissolution-reprecipitation of $CaCO_3$.

The meteoric diagenesis model presented here contains a Cartesian grid in two dimensions, where each cell represents a volumetric geometry of 1 m^3 (Fig. 1A). In each grid cell, the mass and isotopic composition of carbon, oxygen, and calcium are tracked for a fluid and rock phase with constant porosity (Fig. 1B). With each step forward in time, the mass and isotopic compositions of the fluid move between adjacent grid cells according to a prescribed two-dimensional (2-D) divergence-free flow field. During the same time step, mass and isotopic compositions exchange between the rock and fluid phases at a prescribed reaction rate (a free parameter inferred from the duration of exposure). The initial fluid boundary conditions (carbon isotopic composition and concentration) are set to observations from fluids at the top of phreatic zones in modern karst systems (−8‰ $\delta^{13}C$ and 40 ppm total C; Zhao et al., 2015). The advection of each fluid parcel is solved by the continuity equation (Equation 1) with a forward marching Euler numerical scheme.

$$C_{i+1} = C_i - v_i(dt/dy)(C_i - C_{iy}) - u_i(dt/dx)(C_i - C_{ix}), \quad (1)$$

where C_i is the property of interest, such as the $\delta^{13}C$ of the fluid, for a single mesh cell at the current time step, and the i + 1 subscript represents

 Data Repository item 2017034 | doi:10.1130/G38513.1

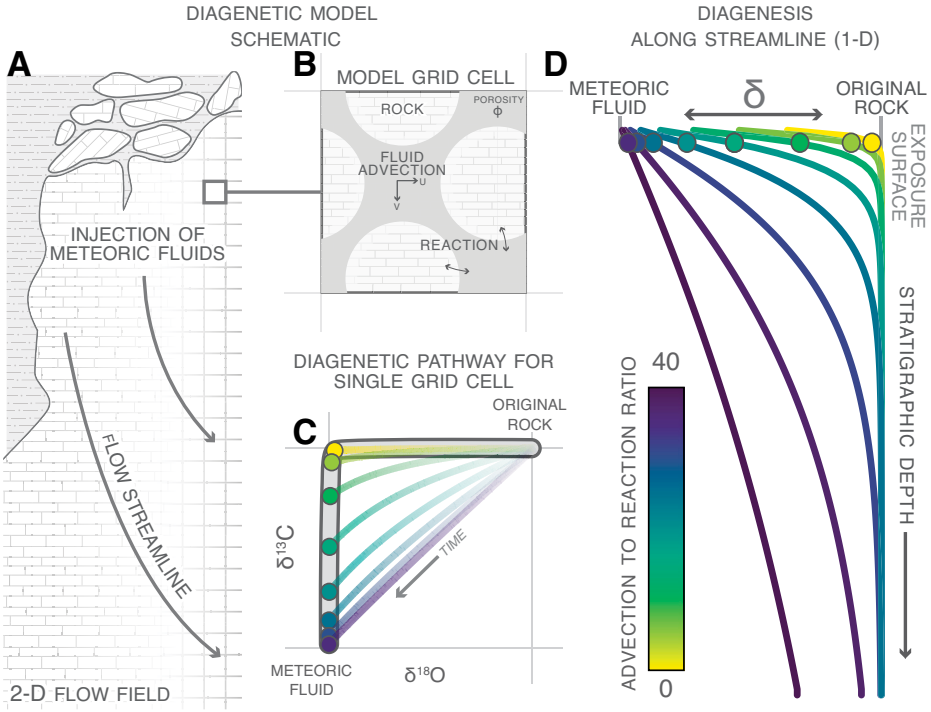

Figure 1. A: Schematic illustration of the components of the diagenetic model of isotopic equilibration between a fluid flowing through a stack of carbonate rocks (2-D—two dimensional). B: The model comprises an interconnected Cartesian set of grid cells. In each cell, the mass and isotopic composition are tracked in a rock phase and fluid phase. C: The coevolution of two elements of interest in a single grid cell depends on the ratio of each element in the fluid, and the relative advection rate of that fluid through the cell. D: This advection to reaction ratio is the primary control on the resulting diagenetic isotopic profile.

the property at one time step (dt) forward. C_{ix} and C_{iy} correspond to the upstream boundary conditions for the mesh cell in the x and y directions, and u and v are the x and y components to the velocity field. The middle Carboniferous isotopic excursions analyzed in this paper have length scales of 10–100 m and likely formed over long time scales (10^5–10^6 yr). Over these time and length scales, diffusion is negligible (Péclet number $\gg$ 1; Berner, 1980).

Laboratory experiments studying fluid-mineral interactions indicate that interfacial dissolution-reprecipitation is the common process driving fluid-mineral equilibration (Putnis and Putnis, 2007; Hellmann et al., 2012). The mass balanced dissolution-reprecipitation reaction step employed by this model (Equation 2) is meant to broadly capture these laboratory observations. The reaction rate constant, R (yr^{-1}), determines the mass flux (F) between the fluid and rock phases. The mass (M) concentrations of carbon, oxygen, and calcium in the rock phase (denoted as subscript j) are set to a stoichiometric calcite composition, and the mass exchange between the rock and fluid is proportional to the mass of each element in the $CaCO_3$ mineral (Equation 3). Essentially, the reaction step represents the dissolution of a small calcite particle followed by the reprecipitation of a new calcite particle of the same mass. The change in the isotopic composition (δ) in the fluid and rock is a function of the total mass exchange between the two phases and the fractionation factor (α) for each element j (Equations 4 and 5). An isotopic fractionation factor (α) for a given element that is equal to 1 corresponds to no isotopic fractionation between the fluid and the rock at equilibrium.

$$(dMd\delta / dt)_{rock} = -(dMd\delta / dt)_{fluid} = F_{in}\delta_{in} - F_{out}\delta_{out}. \quad (2)$$

$$F_{in,j} = F_{out,j} = R \times M_{rock,j}. \quad (3)$$

$$(d\delta / dt)_{rock,j} = \{F_{in,j}[\delta_{fluid,j} + (\alpha_j - 1.0) \times 10^3] - F_{out,j}\delta_{rock,j}\} / M_{rock,j}. \quad (4)$$

$$(d\delta / dt)_{fluid,j} = -\{F_{in,j}[\delta_{fluid,j} + (\alpha_j - 1.0) \times 10^3] - F_{out,j}\delta_{rock,j}\} / M_{fluid,j}. \quad (5)$$

As the infiltrating fluids react with the host rock, a transient reaction front develops and propagates in the direction of flow. This reaction front is the region over which the isotopic compositions of the host rock are transitioning between original isotopic composition and diagenetic fluid isotopic composition. The modeling of mass loss and fluid-rock interactions in porous media by Lichtner (1988) provides a physical basis for understanding the thickness of the reaction front. The thickness of the front is determined by the ratio of mass transport to the ratio of mineral dissolution (mass reaction). The isotope-based model presented in this work captures this phenomenon of a quasi-steady-state reaction front propagating through the rock with a shape that is determined by the ratio of the mass of a given element advecting through the pore space in a fluid to the mass of that same element moving between the fluid and rock phases (Fig. 1D). Regardless of the absolute values chosen for fluid composition, reaction rate, or advection rate, the dimensionless advection to reaction ratio for a specific element of interest (carbon) determines the curvature, magnitude, and length of the diagenetic reaction front for that same element along a single stream line.

FREE PARAMETER ESTIMATION

A probabilistic approach can extract quantitative information (including uncertainty) about the free model parameters from the isotopic data and hundreds of thousands of iterations of the predictive model. With Bayesian inference, probability distributions are provided for each free model parameter (mass advection rate, mass reaction rate, and total duration of diagenesis; see Fig. DR1 in the GSA Data Repository[1]). The inference algorithm updates these distributions to posterior distributions based on the likelihood that the observations (isotopic data and stratigraphic height) could be generated by the predictive model (Metropolis et al., 1953; Hastings, 1970; Patil et al., 2010). Generally, this process involves comparing the observed data set to hundreds of thousands of realizations of the predictive model where the free parameters are selected from the full range of prior distribution values. When the data and model offer little information to constrain a free parameter, the prior and posterior distributions are nearly identical.

[1]GSA Data Repository item 2017034, Figure DR1 and a synthetic test of the Bayesian inference model, is available online at http://www.geosociety.org/pubs/ft2017.htm or on request from editing@geosociety.org.

The only prior information about the free parameters for the middle Carboniferous isotopic data is the maximum duration of diagenesis at Arrow Canyon, Nevada (USA), that is constrained by the age difference in conodonts below and above the unconformity (Fig. 2B; 2.5 ± 1.5 m.y.; Bishop et al., 2009). To represent a lack of prior knowledge about reaction and advection rates, the prior distributions for these free parameters are uniform flat distributions covering five orders of magnitude (Figs. 2C and 2E; 10^{-1}–10^{3}% reaction/m.y. and 10^{-4}–10^{1} m/yr). However, the length scale, curvature, and magnitude of the Arrow Canyon isotopic excursion are only generated by a narrow range of reaction and advection rates (Fig. 2E). In the remaining stratigraphic sections, there is no reliable prior information about the duration of diagenesis, so the posterior distribution for reaction rate inferred from the Arrow Canyon data set (Fig. 2D) is used as a prior distribution for reaction rate in the remaining inference simulations. The resulting posterior distributions of the advection to reaction ratio illustrate the range of values that can predict the chemostratigraphic data with this diagenetic model (Figs. 2A and 2E).

When the inferred duration of diagenesis and the advection to reaction ratio are considered jointly, the carbon isotopic observations from each stratigraphic section may reveal information about the local carbonate weathering. For example, Arrow Canyon has an advection to reaction ratio of ~8, so 8 times more carbon passed through the section than reacted between the fluid and rock. The carbon in this advecting fluid is a mixture of organic carbon (−25‰) and dissolved rock carbon (+2‰) from the overlying vadose and soil zone (Pearson and Hanshaw, 1970; Rightmire and Hanshaw, 1973). The isotopic composition of −8.0‰ $\delta^{13}C$ for the initial fluid is based on observations in the upper portion of modern phreatic fluids in the karst terrain of southeast China (37% of the carbon flux comes from dissolved carbonate; Zhao et al., 2015). This number certainly does not represent the full range of karst fluids in modern or ancient systems, but serves as an estimate of the dissolved carbonate load in terrestrial karst environments. In the Arrow Canyon example, a minimum of 3 m dissolves in the overlying vadose zone every 1 m.y. (37% times the advection to reaction ratio of 8). Therefore, the weathering fluxes from each section are proportional to the advection to reaction ratio, which is determined by the curvature of the isotopic excursion. The lowest inferred weathering rates are in the Strawberry Creek section of the Salt River Range (Wyoming, USA), where at least 0.5–1.5 m of limestone are dissolved per 1 m.y., and the highest weathering flux in Leadville (Colorado, USA; U.S. Geological Survey Core U956) corresponds to the dissolution of 19–80 m of limestone per 1 m.y. (Fig. 2E).

LATE PALEOZOIC GLACIAL-INTERGLACIAL DYNAMICS

High-precision U-Pb zircon ages from interbedded ash layers in late Paleozoic cyclic far-field stratigraphy suggest that ice sheet volume varied at the frequency of long-term eccentricity (400 k.y.; Davydov et al., 2012). Insolation changes at this frequency are small, so there must be a significant positive feedback amplifier that is insensitive to higher frequency insolation changes (<400 k.y.). The drawdown of pCO_2 from the dissolution platform carbonates during lowstands may be such a mechanism.

Carbonate accumulation in the modern interglacial ocean is estimated as 32×10^{12} mol $CaCO_3$/yr (Milliman and Droxler, 1996), and is fixed on long time scales to the volcanic CO_2 input to the atmosphere. The change in carbonate weathering from sea-level highstand to sea-level lowstand can be estimated by extrapolating the dissolution rates calculated from the late Paleozoic carbon isotopic profiles across the entire surface area of shallow-water carbonate platforms. The magnitude of this change is negligible in the modern interglacial ocean (<1% change) because of the limited surface area of shallow-water carbonates (0.6×10^{6} km^2; Walker et al., 2002). This conclusion is supported by observations that the carbonate compensation depth and carbonate accumulation rates did not change significantly from the Last Glacial Maximum through deglaciation (Catubig et al., 1998). However, shallow-water carbonate shelf area was much greater in the late Paleozoic (40×10^{6} km^2; Walker et al., 2002). Consequently, the carbonate weathering flux to the late Paleozoic ocean may have increased 20%–50% whenever sea level fell significantly. If

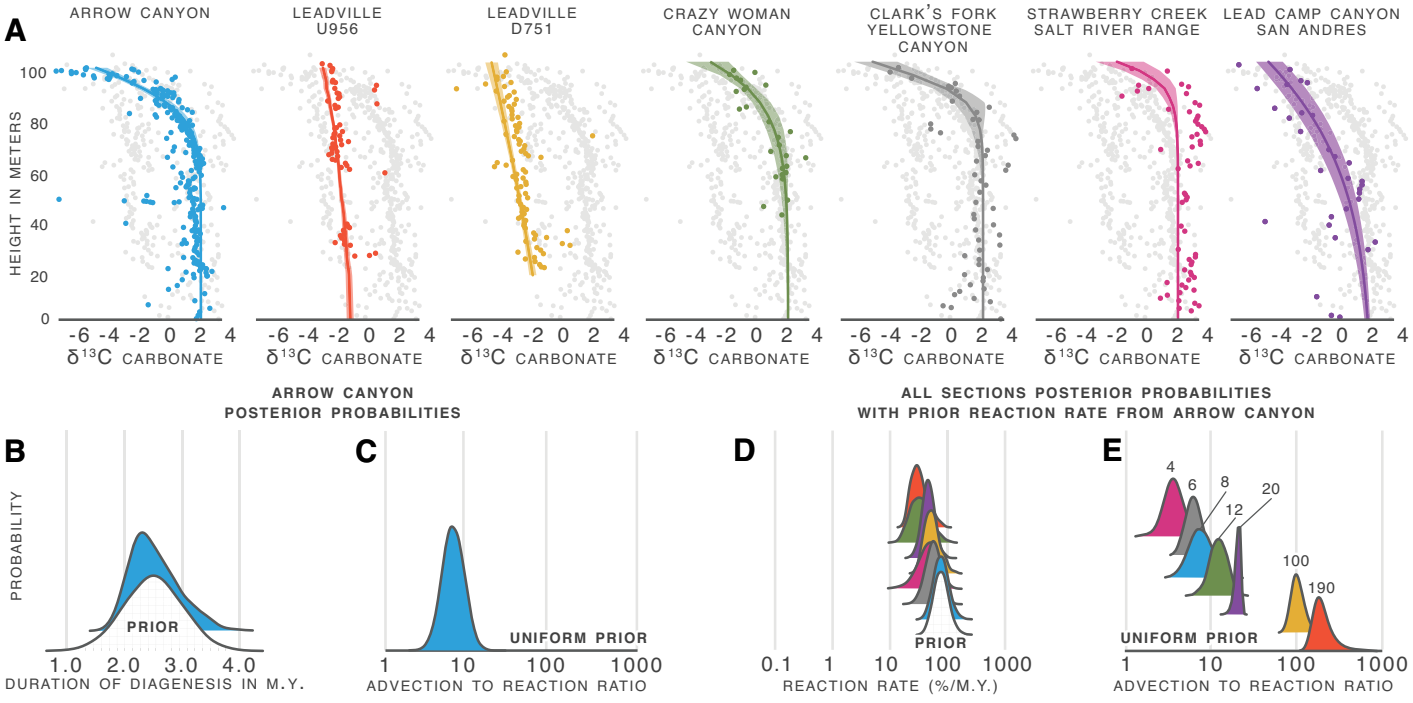

Figure 2. A: Carbon isotopic data from seven middle Carboniferous stratigraphic sections and cores spanning the western United States. Gray data represent all sections, pinned at 100 m to the regional unconformity surface (stratigraphic context and section locations reported by Dyer et al. [2015]). B: Prior and posterior distributions for the duration of diagenesis for the Arrow Canyon (Nevada, USA) data. C: Distributions for the advection to reaction ratio inferred from the Arrow Canyon data. D: Distributions for the reaction rate for each section. E: Distributions of the advection to reaction ratios inferred for each of the stratigraphic data sets depicted in A (colored accordingly).

carbonate accumulation in the ocean is less than the increased flux of dissolved $CaCO_3$, then carbon would move from the atmosphere to the ocean (Sigman and Boyle, 2000), and this loss in atmospheric pCO_2 would result in further cooling and a positive feedback with ice sheet expansion. Moreover, deep-sea carbonate deposition in the modern ocean is dominated by coccolithophores and pelagic foraminifera, which did not evolve until the Triassic, so the lowstand late Paleozoic ocean may have had a lower capacity to redistribute incoming carbonate weathering to the deep ocean (Ridgwell and Zeebe, 2005).

Subsidence or physical erosion of the newly exposed carbonate platforms will cause the carbonate weathering pulse to the ocean to gradually shut off during the lowstand as exposed shelf area decreases and carbonate accumulation and weathering return to steady state. For 100 m of sea-level fall, the carbonate platforms will be exposed for 100 k.y. (typical thermal subsidence rates are 1 mm yr^{-1}; Royden et al., 1980), and the additional drop in pCO_2 over this time scale may shield ice sheets from higher frequency orbital-driven changes in insolation. Therefore, the complex feedbacks among carbonate weathering, glacioeustasy, and subsidence may have had as-yet unknown roles in the climate variability during the late Paleozoic ice age.

ACKNOWLEDGMENTS

Dyer, Maloof, and Higgins were supported by the Scott Vertebrate Paleontology Fund, Princeton University. We thank the reviewers for their constructive criticism that significantly improved the quality of this publication.

REFERENCES CITED

Allan, J., and Matthews, R., 1982, Isotope signatures associated with early meteoric diagenesis: Sedimentology, v. 29, p. 797–817, doi:10.1111/j.1365-3091.1982.tb00085.x.

Berner, R.A., 1980, Early diagenesis: A theoretical approach: Princeton, New Jersey, Princeton University Press, 256 p.

Bishop, J.W., Montañez, I.P., Gulbranson, E.L., and Brenckle, P.L., 2009, The onset of mid-Carboniferous glacio-eustasy: Sedimentologic and diagenetic constraints, Arrow Canyon, Nevada: Palaeogeography, Palaeoclimatology, Palaeoecology, v. 276, p. 217–243, doi:10.1016/j.palaeo.2009.02.019.

Bögli, A., and Schmid, J.C., 1980, Karst hydrology and physical speleology: Berlin, Springer-Verlag, 286 p., doi:10.1007/978-3-642-67669-7.

Budd, D.A., 1988, Aragonite-to-calcite transformation during freshwater diagenesis of carbonates: Insights from pore-water chemistry: Geological Society of America Bulletin, v. 100, p. 1260–1270, doi:10.1130/0016-7606(1988)100<1260:ATCTDF>2.3.CO;2.

Catubig, N.R., Archer, D., Francois, R., Demenocal, P., Howard, W., and Yu, E.-F., 1998, Global deep-sea burial rate of calcium carbonate during the Last Glacial Maximum: Paleoceanography, v. 13, p. 298–310, doi:10.1029/98PA00609.

Davydov, V., Korn, D., and Schmitz, M., 2012, The Carboniferous Period, *in* Gradstein, F., et al., The geologic time scale 2012: Boston, Amsterdam, Elsevier, p. 603–652.

Dyer, B., Maloof, A.C., and Higgins, J.A., 2015, Glacioeustasy, meteoric diagenesis, and the carbon cycle during the Middle Carboniferous: Geochemistry, Geophysics, Geosystems, v. 16, p. 3383–3399, doi:10.1002/2015GC006002.

Hastings, W.K., 1970, Monte Carlo sampling methods using Markov chains and their applications: Biometrika, v. 57, p. 97–109, doi:10.1093/biomet/57.1.97.

Hayes, J.M., Strauss, H., and Kaufman, A.J., 1999, The abundance of ^{13}C in marine organic matter and isotopic fractionation in the global biogeochemical cycle of carbon during the past 800 Ma: Chemical Geology, v. 161, p. 103–125, doi:10.1016/S0009-2541(99)00083-2.

Hellmann, R., Wirth, R., Daval, D., Barnes, J.-P., Penisson, J.-M., Tisserand, D., Epicier, T., Florin, B., and Hervig, R.L., 2012, Unifying natural and laboratory chemical weathering with interfacial dissolution-reprecipitation: A study based on the nanometer-scale chemistry of fluid-silicate interfaces: Chemical Geology, v. 294–295, p. 203–216, doi:10.1016/j.chemgeo.2011.12.002.

James, N.P., and Choquette, P.W., 1984, Diagenesis 9. Limestones—The meteoric diagenetic environment: Geoscience Canada, v. 11, p. 161–194.

Lichtner, P.C., 1988, The quasi-stationary state approximation to coupled mass transport and fluid-rock interaction in a porous medium: Geochimica et Cosmochimica Acta, v. 52, p. 143–165, doi:10.1016/0016-7037(88)90063-4.

Lohmann, K.C., 1988, Geochemical patterns of meteoric diagenetic systems and their application to studies of paleokarst, *in* James, N.P., and Choquette, P.W., eds., Paleokarst: New York, Springer-Verlag, p. 58–80, doi:10.1007/978-1-4612-3748-8_3.

Matthews, R., 1974, A process approach to diagenesis of reefs and reef associated limestones, *in* Laporte, L.F., ed., Reefs in time and space: Society of Economic Paleontologists and Mineralogists Special Publication 18, p. 234–256, doi:10.2110/pec.74.18.0234.

Metropolis, N., Rosenbluth, A.W., Rosenbluth, M.N., Teller, A.H., and Teller, E., 1953, Equation of state calculations by fast computing machines: Journal of Chemical Physics, v. 21, p. 1087–1092, doi:10.1063/1.1699114.

Milliman, J., and Droxler, A., 1996, Neritic and pelagic carbonate sedimentation in the marine environment: Ignorance is not bliss: Geologische Rundschau, v. 85, p. 496–504, doi:10.1007/BF02369004.

Patil, A., Huard, D., and Fonnesbeck, C.J., 2010, PyMC: Bayesian stochastic modelling in Python: Journal of Statistical Software, v. 35, p. 1, doi:10.18637/jss.v035.i04.

Pearson, F., and Hanshaw, B., 1970, Sources of dissolved carbonate species in groundwater and their effects on ^{14}C dating: Isotope Hydrology, v. 1970, p. 271–286.

Plummer, L.N., Vacher, H.L., Mackenzie, F.T., Bricker, O.P., and Land, L.S., 1976, Hydrogeochemistry of Bermuda: A case history of ground-water diagenesis of biocalcarenites: Geological Society of America Bulletin, v. 87, p. 1301–1316, doi:10.1130/0016-7606(1976)87<1301:HOBACH>2.0.CO;2.

Putnis, A., and Putnis, C.V., 2007, The mechanism of reequilibration of solids in the presence of a fluid phase: Journal of Solid State Chemistry, v. 180, p. 1783–1786, doi:10.1016/j.jssc.2007.03.023.

Ridgwell, A., and Zeebe, R.E., 2005, The role of the global carbonate cycle in the regulation and evolution of the Earth system: Earth and Planetary Science Letters, v. 234, p. 299–315, doi:10.1016/j.epsl.2005.03.006.

Rightmire, C.T., and Hanshaw, B.B., 1973, Relationship between the carbon isotope composition of soil CO_2 and dissolved carbonate species in groundwater: Water Resources Research, v. 9, p. 958–967, doi:10.1029/WR009i004p00958.

Royden, L., Sclater, J., and Von Herzen, R., 1980, Continental margin subsidence and heat flow: Important parameters in formation of petroleum hydrocarbons: American Association of Petroleum Geologists Bulletin, v. 64, p. 173–187.

Sigman, D.M., and Boyle, E.A., 2000, Glacial/interglacial variations in atmospheric carbon dioxide: Nature, v. 407, p. 859–869, doi:10.1038/35038000.

Swart, P.K., and Eberli, G., 2005, The nature of the $\delta^{13}C$ of periplatform sediments: Implications for stratigraphy and the global carbon cycle: Sedimentary Geology, v. 175, p. 115–129, doi:10.1016/j.sedgeo.2004.12.029.

Thrailkill, J., 1968, Chemical and hydrologic factors in the excavation of limestone caves: Geological Society of America Bulletin, v. 79, p. 19–46, doi:10.1130/0016-7606(1968)79[19:CAHFIT]2.0.CO;2.

Veizer, J., et al., 1999, $^{87}Sr/^{86}Sr$, $\delta^{13}C$ and $\delta^{18}O$ evolution of Phanerozoic seawater: Chemical Geology, v. 161, p. 59–88, doi:10.1016/S0009-2541(99)00081-9.

Walker, L.J., Wilkinson, B.H., and Ivany, L.C., 2002, Continental drift and Phanerozoic carbonate accumulation in shallow-shelf and deep-marine settings: Journal of Geology, v. 110, p. 75–87, doi:10.1086/324318.

Whitaker, F.F., and Smart, P.L., 2007, Geochemistry of meteoric diagenesis in carbonate islands of the northern Bahamas: 1. Evidence from field studies: Hydrological Processes, v. 21, p. 949–966, doi:10.1002/hyp.6532.

Zhao, M., Liu, Z., Li, H.-C., Zeng, C., Yang, R., Chen, B., and Yan, H., 2015, Response of dissolved inorganic carbon (DIC) and $\delta^{13}C_{DIC}$ to changes in climate and land cover in SW China karst catchments: Geochimica et Cosmochimica Acta, v. 165, p. 123–136, doi:10.1016/j.gca.2015.05.041.

Manuscript received 23 August 2016
Revised manuscript received 1 November 2016
Manuscript accepted 2 November 2016

Printed in USA